applied sciences

MDPI

Article

Preliminary Study on the Model of Thermal Laser Stimulation for Defect Localization in Integrated Circuits

Han Yang [1,2], Rui Chen [1,2,*], Jianwei Han [1,2], Yanan Liang [1], Yingqi Ma [1,2] and Hao Wu [1,3]

[1] National Space Science Center, Chinese Academy of Sciences, Beijing 100190, China; yanghan18@mails.ucas.ac.cn (H.Y.); hanjw@nssc.ac.cn (J.H.); liangyanan@nssc.ac.cn (Y.L.); myq@nssc.ac.cn (Y.M.); wuhao192@mails.ucas.ac.cn (H.W.)

[2] School of Astronomy and Space Science, University of Chinese Academy of Sciences, Beijing 100049, China

[3] School of Electronic, Electrical and Communication Engineering, University of Chinese Academy of Sciences, Beijing 100049, China

* Correspondence: chenrui2010@nssc.ac.cn

Received: 1 November 2020; Accepted: 25 November 2020; Published: 30 November 2020



Abstract: Thermal Laser Stimulation (TLS) is an efficient technology for integrated circuit defect localization in Failure Analysis (FA) laboratories. It contains Optical Beam-Induced Resistance Change (OBIRCH), Thermally-Induced Voltage Alteration (TIVA), and Seebeck Effect Imaging (SEI). These techniques respectively use the principle of laser-induced resistance change and the Seebeck effect. In this paper, a comprehensive model of TLS technology is proposed. Firstly, the model presents an analytical expression of the temperature variation in Integrated Circuits (IC) after laser irradiation, which quantificationally shows the positive correlation with laser power and the negative correlation with scanning velocity. Secondly, the model describes the opposite influence of laser-induced resistance change and the Seebeck effect in the device. Finally, the relationship between the current variation measured in the experiment and other parameters, especially the voltage bias, is well explained by the model. The comprehensive model provides theoretical guidance for the efficient and accurate defect localization of TLS technology.

Keywords: TLS; OBIRCH; SEI; Seebeck effect; TIVA; TCR; Seebeck coefficient

1. Introduction

With the scaling down of the integrated circuit process and the increase of the metal layers, circuit-level defects are more and more difficult for an optical microscope to observe. Therefore, nondestructive Failure Analysis (FA) for Integrated Circuits (IC) has gradually become necessary. Defect localization is a fundamental step in FA. Accurate and efficient localization makes a great contribution to the analysis of the failure's physical causes. At present, several optical based technologies, such as Emission Microscopy (EMMI), Photoelectric Laser Stimulation (PLS), Thermal Laser Stimulation (TLS), and Laser Voltage Probing (LVP), have been proven to meet the present requirements [1]. Among all the advanced technology, TLS is an efficient and non-destructive method used in back-side localization [2–4]. TLS technology has proved that it is sensitive to leakage current [5], short-circuit [3], and open-circuit [6]. It is applicable to metallic, polysilicon, and highly doped silicon structures [7]. However, TLS still has some limitations. Because of the high reflectivity of the metal layer to the laser, it is difficult for TLS to locate a defect at a deep level [8]. In 2017, a modified technology called Lock-in TLS was proposed to locate the defect in multilevel interconnects [9].

TLS technology contains three techniques, Optical Beam-Induced Resistance Change (OBIRCH), Thermally-Induced Voltage Alteration (TIVA), and the Seebeck Effect Imaging (SEI). OBIRCH was

firstly proposed by Nikawa et al. [10], while TIVA and SEI were proposed by Edward I. Cole Jr. [11]. A simulation model of OBIRCH and TIVA was proposed in 2001 [12]. In 2005, reports showed that the SEI signal would be affected by the OBIRCH signal in experiments [13,14]. The three techniques mentioned above are used in different test situations. Each technique has its unique test mechanism. However, the comprehensive theoretical model of TLS technology is still deficient.

In this paper, a comprehensive model of TLS technology is proposed. This model describes the whole process of the laser beam interacting with the IC and the joint influence of the laser-induced resistance change effect and Seebeck effect. Next, a defect localization and analysis experiment is carried out. The experimental results are consistent with the predictions of the theoretical model. The comprehensive model provides theoretical guidance for the efficient and accurate defect localization of TLS technology.

2. TLS Principle

2.1. Classical Model

Because of the reflection of the front-side metal layer, it is difficult for the laser to reach deep levels from the front side of the device. Backside laser irradiation has proven to be an effective method [8,11]. In TLS, a continuous infrared laser (wavelength of 1.3 µm) is used to scan the back-side silicon substrate for two reasons,

- The photon's energy for the 1.3 µm infrared laser ($\frac{hc}{\lambda} \sim 0.95$ eV) is lower than the silicon band gap energy (1.12 eV), so the laser hardly generates a photo-current [10];
- Silicon is almost transparent at such a wavelength, so the laser beam can reach the active area through the back-side substrate at low loss [11].

It is well known that thermal energy leads to an increasing temperature ΔT, causing a variation of resistivity:

$$\Delta\rho = \rho_0 \left(\alpha_{\mathrm{TCR}} - 2\delta_r\right) \Delta T \tag{1}$$

where ρ_0, α_{TCR}, and δ_r are respectively the electrical resistivity, the Thermal Coefficient of Resistivity (TCR), and the thermal expansion coefficient of the material. δ_r is so small relative to α_{TCR} that it is negligible in most cases [15]. The resistivity and temperature coefficients of some metal materials are shown in Table 1.

Table 1. Resistivity and temperature coefficients of some metal materials [16].

Material	ρ_0(20 °C) (Ω · m)	α_{TCR} (°C^{-1})
Al	2.9×10^{-8}	4.3×10^{-3}
Cu	1.7×10^{-8}	3.9×10^{-3}

In the OBIRCH technique, a constant voltage bias V_0 is applied to the Device Under Test (DUT) [12]. Due to the changed resistance, the current ΔI varies as:

$$\Delta I \equiv -\frac{\Delta R}{R} I = -\frac{\Delta R}{R^2} V_0 \tag{2}$$

where ΔR is the resistance variation and I is the current of the DUT before laser irradiation. In the TIVA technique, however, a constant current bias I_0 is used [12]. The variation of the voltage ΔV is:

$$\Delta V \equiv \frac{\Delta R}{R} V = I_0 \Delta R \tag{3}$$

where V is the voltage of the DUT before laser irradiation.

The SEI technique, which typically uses zero-bias or constant current bias, is based on the so-called Seebeck effect. While two contiguous materials have different temperatures (see Figure 1) [7], a Seebeck voltage is generated according to the following equation:

$$\Delta V_S \equiv (S_1 - S_2)\,\Delta T = S_{1-2}\Delta T \tag{4}$$

where ΔT is the temperature difference between two materials and $S_{1-2} = \frac{dV}{dT}$ is the Seebeck coefficient. Seebeck coefficients for several materials or junctions are presented in Table 2. It can be positive or negative in different contacted materials. The Seebeck voltage is independent of the circuit resistance, and it has an effect on the voltage or current of the circuit.

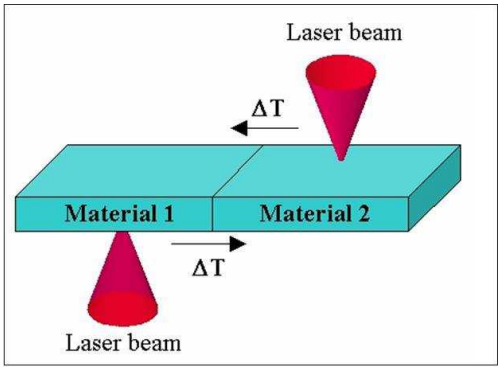


Figure 1. Seebeck effect principle. A Seebeck voltage is generated due to the temperature difference of the two contiguous materials.

Table 2. Seebeck coefficients for several materials and junctions [16].

Material or Junction	S_{1-2} (μV/K)
Al	−3.5 *
W	3.6 *
Al/n + Si	287 **
Al/p + Si	−202 **

* Measured relative to copper, ** relative thermoelectric power for a 10^{18} cm^{-3} doping.

2.2. Comprehensive Model

The rationales for all three techniques have been proposed; however, these effects occur simultaneously in the circuit, and the results they produce interfere with each other. Therefore, it is necessary to establish a comprehensive model of TLS technology to research for the proportion of each effect on the circuit.

2.2.1. The Evolution of the Temperature Field in the Circuit after Laser Irradiation

When the laser beam is focused on the active area of the DUT (see Figure 2), a temperature field is generated, following the thermal conduction equation:

$$\rho c \frac{\partial T}{\partial t} - \kappa \nabla^2 T = Q(x, y, z, t) \tag{5}$$

where ρ, c, and κ are respectively the density, heat capacity, and thermal conductivity of the material. $Q(x, y, z, t)$, as a function of position (x, y, z) and time t, is the heating source produced by the laser beam. Taking the case of a laser beam moving along the positive x direction as an example, the expression of Q is:

$$Q(x,y,z,t) = \frac{(1-R)P_0}{\pi\gamma\omega^2(z)} \exp\left[-\frac{(x-vt)^2+y^2}{\omega^2(z)} - \frac{z}{\gamma}\right] \tag{6}$$

where P_0, $\omega^2(z)$, R, and γ are respectively the power, spot size, reflectivity, and attenuation length of the laser. v is the scanning velocity of the laser spot. Equation (6) uses the approximation of the Gaussian intensity profile [15].

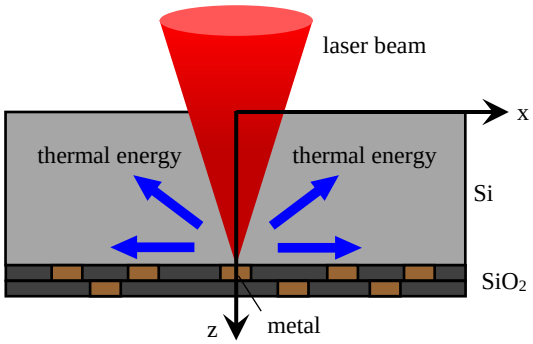


Figure 2. Laser beam focused on the metal layer. The thermal energy will diffuse in all directions.

In general, the temperature variation in the xy plane is what we are interested in. Besides, the area of the IC layout is much larger than that of the laser spot. Therefore, the model mentioned above can be transformed into the temperature field distribution in two-dimensional infinite space. Equations (5) and (6) are converted to:

$$\rho c\frac{\partial T}{\partial t} - \kappa\left(\frac{\partial^2 T}{\partial x^2} + \frac{\partial^2 T}{\partial y^2}\right) = Q(\vec{r},t) \tag{7}$$

$$Q(\vec{r},t) = \frac{(1-R)P_0}{\pi\gamma\omega^2} \exp\left[-\frac{(x-vt)^2+y^2}{\omega^2}\right] \tag{8}$$

where $\vec{r} = (x,y)$. In Equation (8), the laser spot size ω^2 is treated as a constant. Considering that the temperature difference $\Delta T = T - T_0$ is also a special solution to Equation (7), the boundary condition is:

$$\Delta T(\vec{r},t)\big|_{|\vec{r}|\to\infty} = 0,\ \Delta T(\vec{r},t)\big|_{t=0} = 0 \tag{9}$$

Equation (7) can be solved by a Green's function approach [17] to give:

$$\Delta T(\vec{r},t) = \int_0^t \mathrm{d}t' \iint_\Sigma G(\vec{r},t;\vec{r}',t')Q(\vec{r}',t')\mathrm{d}\vec{r}' \tag{10}$$

where Σ is the whole two-dimensional plane and $G(\vec{r},t;\vec{r}',t')$ is the Green's function for point excitation at $(\vec{r}',t')$ given by:

$$G(\vec{r},t;\vec{r}',t') = \frac{1}{4\pi k\,(t-t')} \exp\left[-\frac{(x-x')^2+(y-y')^2}{4k\,(t-t')}\right]\eta(t-t') \tag{11}$$

where $k = \frac{\kappa}{\rho c}$ and $\eta(t-t')$ is the step (Heaviside) function. Using Equations (8) and (11) in Equation (10), we can obtain:

$$\Delta T(\vec{r},t) = \frac{(1-R)P_0}{4\pi\rho c\gamma} \int_0^t \frac{1}{\omega^2 + 4k\,(t-t')} \exp\left[-\frac{(x-vt')^2+y^2}{\omega^2+4k\,(t-t')}\right]\mathrm{d}t' \tag{12}$$

2.2.2. The Variation of the Current or Voltage in the Circuit

When the laser beam is focused on the abnormal spot or the normal spot of the DUT, a temperature variation ΔT that meets Equation (12) is formed. The variation of resistance ΔR and the Seebeck voltage ΔV_S are respectively:

$$\Delta R = \int \Delta\rho \frac{\mathrm{d}l}{A} = \int \rho_0 \alpha_{TCR} \frac{\Delta T}{A} \mathrm{d}l \tag{13}$$

and:

$$\Delta V_S = \int S_{1-2} \nabla(\Delta T) \cdot \mathrm{d}\vec{l}_{1-2} \tag{14}$$

where $\mathrm{d}l_{1-2}$ is a tiny length in the direction of the current flowing, A is the cross-sectional area, and $\nabla(\Delta T) \cdot \mathrm{d}\vec{l}_{1-2}$ is the temperature difference between the two contact materials. At the abnormal spot of the failed device, thermal diffusion is more difficult, so the local temperature is much higher. Therefore, the values of ΔR and ΔV_S are bigger than those at the normal spot. The difference can be detected by testing the current or voltage.

As for a device under constant voltage bias V_0, ΔR and ΔV_S will cause a variation of the current. The value of current variation ΔI is:

$$\Delta I = I_{TLS} - I = \frac{V_0 + \Delta V_S}{R + \Delta R} - \frac{V_0}{R} \tag{15}$$

where V_0 is the voltage bias, I_0 is the current before the laser irradiation starts, and R is the resistance of the DUT [14]. The laser power used in the experiment is less than 100 mW, resulting in very small ΔR and ΔV_S. Therefore, Equation (15) is approximated to:

$$\Delta I = \frac{\Delta V_S}{R + \Delta R} + \left(\frac{V_0}{R + \Delta R} - \frac{V_0}{R} \right) \approx \frac{\Delta V_S}{R} - \frac{V_0}{R^2} \Delta R \tag{16}$$

There are two parts on the right of Equation (16), the first of which is mainly contributed by the Seebeck effect, and the second is dominated by laser-induced resistance change. Therefore, the OBIRCH and SEI techniques coexist in a test. While V_0 is equal to a critical value V_c, ΔI will be equal to zero. From Formula (16), the value of V_c is:

$$V_c = \frac{\Delta V_S}{\Delta R} R \tag{17}$$

When $V_0 > V_c$, $\Delta I < 0$, that is the OBIRCH technique dominates. Otherwise, the SEI dominates.

While constant current bias I_0 is applied, the TIVA and SEI will coexist, and the voltage variation ΔV is:

$$\Delta V = V_{TLS} - V = [I_0 (R + \Delta R) - \Delta V_S] - I_0 R = -\Delta V_S + I_0 \Delta R \tag{18}$$

The contributions of the two effects are still opposite. Besides, a critical current bias I_c that causes $\Delta I = 0$ is [14]:

$$I_c = \frac{\Delta V_S}{\Delta R} \tag{19}$$

When $I_0 > I_c$, $\Delta V > 0$, and the TIVA technique dominates. When $I_0 < I_c$, the SEI dominates. Therefore, the SEI technique always requires low bias conditions.

For an active device, according to [14], an extra weak current I_{PN} exists after laser irradiation, which is preliminarily interpreted as a light-current signal. I_{PN} has little influence on the current variation ΔI or voltage variation ΔV.

2.2.3. The Comprehensive Model

Combining the conclusions of Sections 2.2.1 and 2.2.2, the relationship between the values measured in TLS technology and the experimental parameters is established. In constant voltage bias, the current variation is:

$$\Delta I \approx \frac{C_1 P_0}{R} \int S_{1-2} \nabla f(x, y, v, t) \cdot \mathrm{d}\vec{l}_{1-2} - \frac{C_1 P_0 V_0}{R^2} \int \frac{\rho_0 \alpha_{\mathrm{TCR}}}{A} f(x, y, v, t) \mathrm{d}l \tag{20}$$

In constant voltage bias, the voltage variation is:

$$\Delta V = -C_1 P_0 \int S_{1-2} \nabla f(x, y, v, t) \cdot \mathrm{d}\vec{l}_{1-2} + C_1 P_0 I_0 \int \frac{\rho_0 \alpha_{\mathrm{TCR}}}{A} f(x, y, v, t) \mathrm{d}l \tag{21}$$

where:

$$C_1 = \frac{1-R}{4\pi\rho c\gamma}, \; f(x, y, v, t) = \int_0^t \frac{1}{\omega^2 + 4k\,(t-t')} \exp\left[-\frac{(x - vt')^2 + y^2}{\omega^2 + 4k\,(t-t')}\right] \mathrm{d}t' \tag{22}$$

The meaning of each consideration is already explained in the content above. Equations (20) and (21) entirely describe the principle of TLS technology. They correlate the measurable quantities (current variation ΔI and voltage variation ΔV) with adjustable quantities (laser power P_0, scanning velocity v, and bias conditions V_0/I_0).

The structure and material composition of actual ICs are complex. Therefore, the evolution of the temperature field with time also varies with different materials and structures. However, the predictions of the comprehensive model are still in good agreement with the experimental results.

3. Experiment and Discussion

3.1. Experiment Setup

3.1.1. Testing System

In order to verify the comprehensive model, a defect localization experiment is performed using the Laser Scanning and Testing System (LSTS; see Figure 3) at the National Space Science Center, Chinese Academy of Sciences. The relevant parameters of the facility are shown in Table 3. The computer is used to monitor the current. As the laser beam scans the defect location, the abnormal ΔI will be tested, and a red spot will be marked on the layout diagram. The test results supplied by the voltage source or current source have similar properties according to Equations (16) and (18), so a voltage source is used for the test.

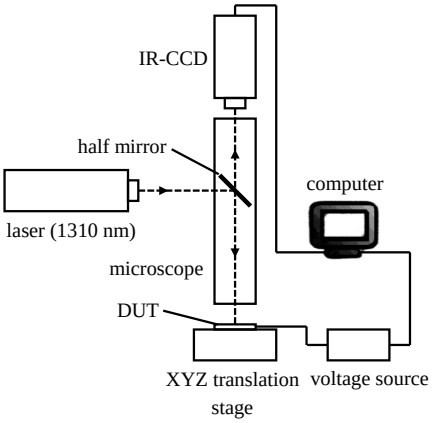


Figure 3. Schematic diagram of the Laser Scanning and Testing System (LSTS). The voltage source is used to supply the DUT, and the computer is used to monitor the current. As the laser beam scans the defect location, the abnormal ΔI will be tested, and a red spot will be marked on the layout diagram, which is imaged by the IR-CCD.

Table 3. Relevant parameters of the LSTS.

laser	Wavelength	1310 nm
	Power	0~100 mW
Translation Stage	Scanning Speed	0~100 mm/s
	Positioning Accuracy	0.1 μm

3.1.2. DUT

The tested device sample is a Micro Control Unit (MCU; see Figure 4a), which is a computer system integrated on a chip. After functional testing, the failure area is located in the red box in Figure 4a. When the normal sample is power supplied with no function running, the supply voltage V_0 is situated in the range of 1.8~3.6 V. The typical value of the current I_0 is 1.4 μA when V_0 = 3.3 V.

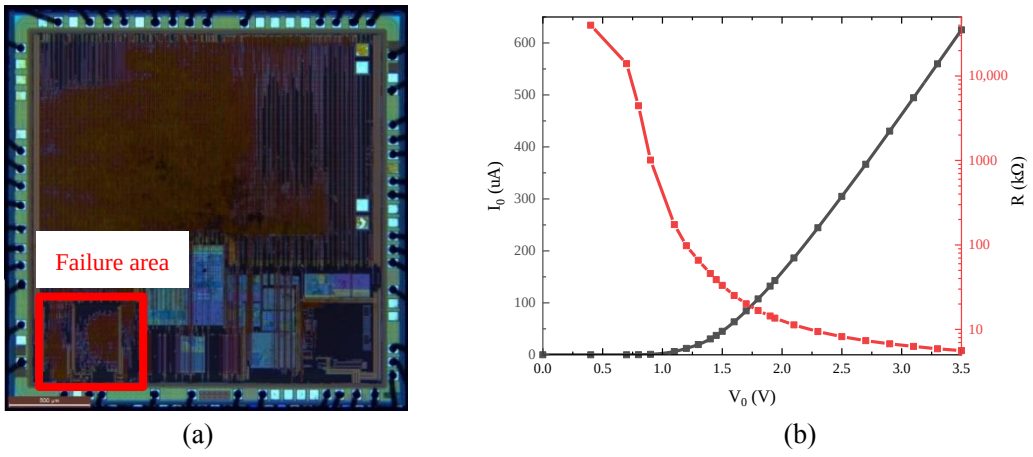


Figure 4. Characteristics of the failed sample: (**a**) front-side optical image of the MCU sample and the location of the failure area; (**b**) I-V and R-V curves.

The fail sample has a leakage current (Figure 4b), the typical value of which is I_0 = 595 μA at V_0 = 3.3 V. This current value is much larger than that of the normal device. As the supplied voltage increases, the current increases, and the resistance decreases.

3.2. Results and Discussion

3.2.1. Failure Localization

When V_0 is set at 3.5 V, the current of the sample I_0 is 626 µA. According to the back-side CCD image (Figure 5a), the size of the sample is 2450 µm × 2450 µm. Set the lower-left corner of the chip as the origin of the coordinates, the horizontal direction as the X-axis, and the vertical direction as the Y-axis (Figure 5a). After laser-scanning with a 40 mW laser beam, the abnormal spot is determined, and the coordinates are (X_{fail} = 2064 µm, Y_{fail} = 2033 µm) (Figure 5b). The abnormal current variation at the abnormal spot is about 2.5 µA, while the current variation at the normal spot is about 0.5 µA (Figure 5c). This result is in accordance with the result tested by Emission Microscopy (EMMI) (Figure 6), which is another common defect localization technology [18]. Figure 7 shows a possible physical reason for the failure, that is a cavity in the copper, found by the Focused Ion Beam (FIB) facility.

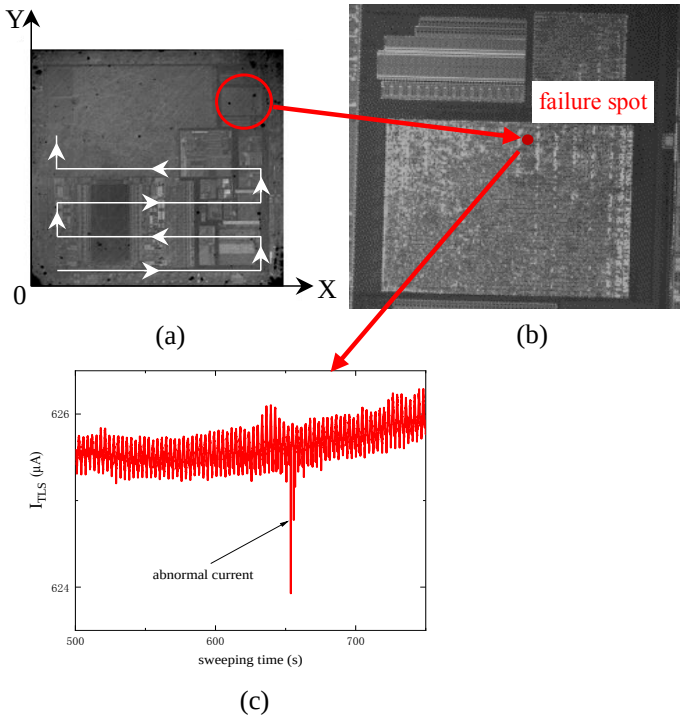
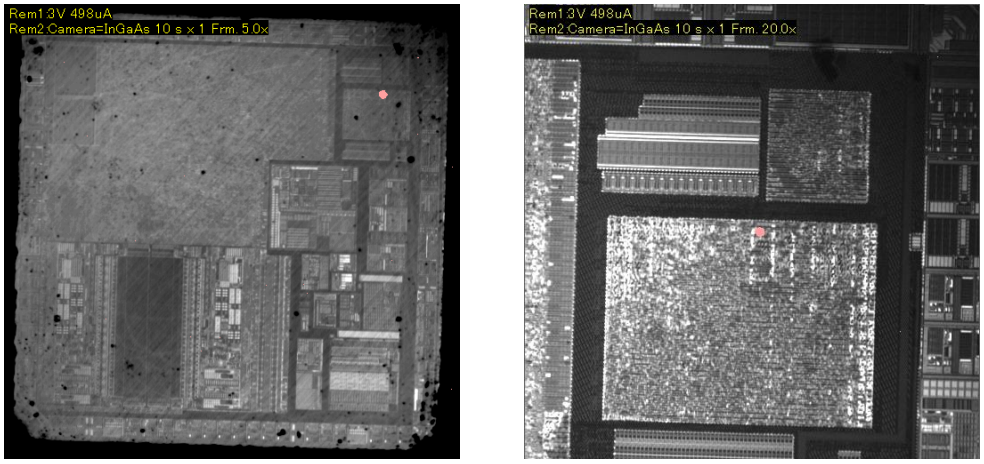


Figure 5. Localization of the abnormal spot using the LSTS: (**a**) The back-side CCD image of the DUT. The scanning scheme is shown by the white line and arrow. (**b**) While the laser is scanning the abnormal spot, an abnormal current is tested by the current meter, and a red spot is marked on the failure spot. (**c**) The abnormal current variation is about 2.5 µA, while the normal current variation is about 0.5 µA.



(a) (b)

Figure 6. Defect localization by Emission Microscopy (EMMI). The voltage is set at 3 V. An InGaAs IR-camera is used for imaging: (**a**) the magnification is 5.0×; (**b**) the magnification is 20.0×.

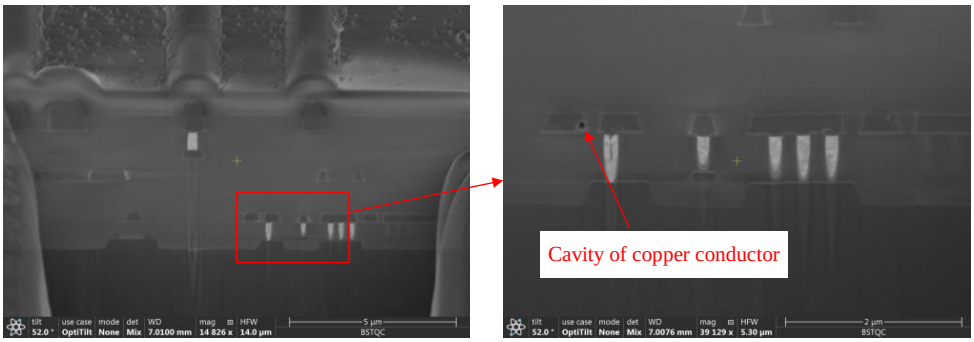


Figure 7. Cavity of the copper conductor found by the Focused Ion Beam (FIB), which is probably the physical cause of the failure.

3.2.2. The Relationship between Current Variation and Laser Power and Scanning Velocity

Figure 8 shows the relationship between current variation and laser power and scanning velocity at the abnormal spot. A constant voltage bias set at 3.5 V is used. Figure 8 also shows the maximum ΔT during laser irradiation as a function of laser power and scanning velocity at $(x = 0, y = 0)$ according to Equation (12). The experimental results meet these two conclusions based on the positive ratio of ΔT and ΔI.

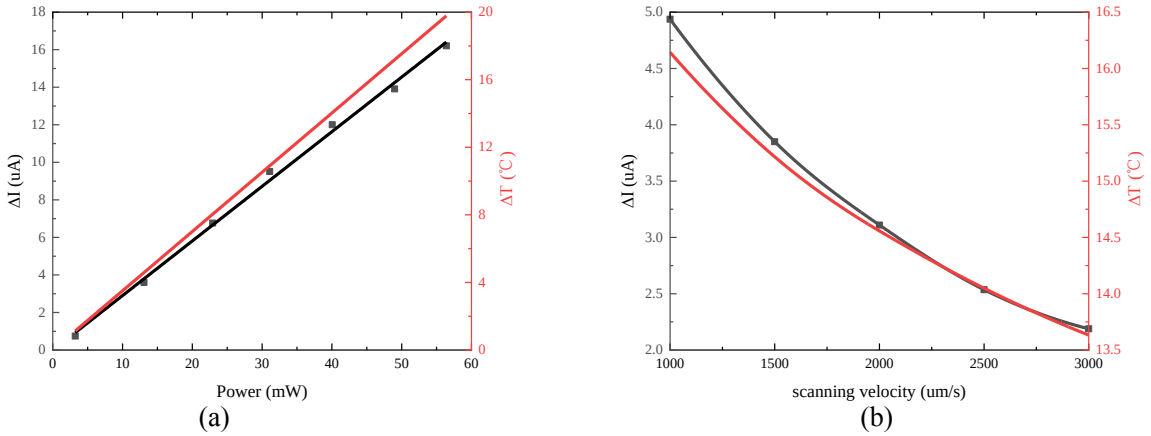


Figure 8. Comparison of the current variation ΔI in the experiment and temperature variation ΔT in the comprehensive model. ΔT is calculated through Equation (12) using the data in [16]. (**a**) The laser power varies while the scanning velocity is set at 2500 μm/s. (**b**) The scanning velocity varies while the laser power is set at 40 mW.

3.2.3. Response Time for Laser Irradiation

As mentioned above, the evolution of the temperature field with time varies with different materials and structures. This can also be semi-quantitatively explained by the comprehensive model. As a comparison, Points A (abnormal spot) and B (normal spot, $x_A - x_B = 100$ μm, $y_A - y_B = 0$ μm) in Figure 9, are selected for laser irradiation testing. Several typical bias voltages are selected to test the response of the current variation (Figure 10a,b). The positive or negative value of the current variation will be discussed in Section 3.2.4.

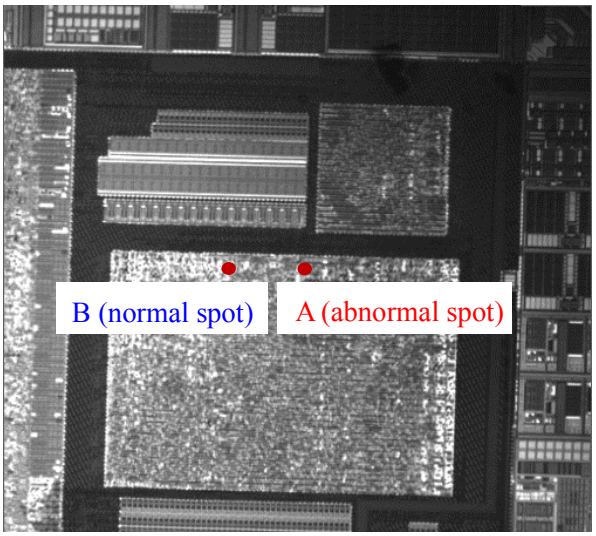


Figure 9. Two selected spots for laser irradiation testing. The laser will continuously irradiate Point A or Point B.

Due to Equation (12), when the scanning velocity is zero, the temperature variation at the location $(x = 0, y = 0)$ is:

$$\Delta T(0,t) = \frac{(1-R)P_0}{4\pi\rho c\gamma}\int_0^t \frac{\mathrm{d}t'}{\omega^2 + 4k(t-t')} = \frac{(1-R)P_0}{16\pi\kappa\gamma}\ln\left(1+\frac{4kt}{\omega^2}\right) \quad (23)$$

Although Equation (23) shows that the temperature always increases with laser irradiation time, the increase is very slow after a long time. This is consistent with the pattern shown in Figure 10. Besides, From Equation (20), the current variation is proportional to ΔT. The response time at the

abnormal spot (less than 100 ms) is much less than that at the normal spot (more than 1 s). This is caused by the different materials and structures in the DUT. The material at the abnormal spot is metal Cu with extremely high thermal conductivity, so $k = \frac{\kappa}{\rho c}$ is relatively large. However, the material at the normal spot is the insulation material with low κ, causing the small k.

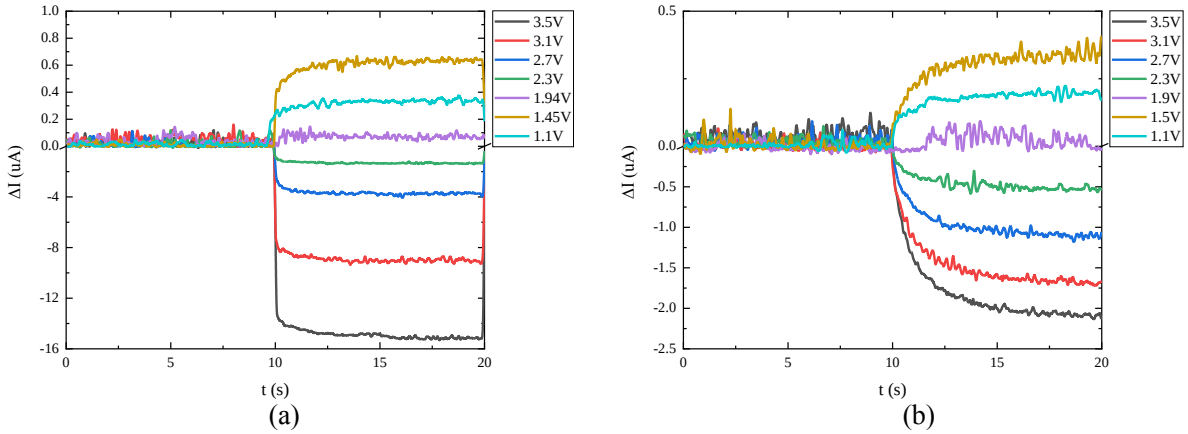


Figure 10. Curve of the current variation and the irradiation time at different bias voltages V_0. The laser beam starts to irradiate at t = 10 s with no scanning velocity. The laser power is set at 40 mW: (**a**) Point A (abnormal spot); (**b**) Point B (normal spot).

In addition, according to Equation (16), the OBIRCH technique dominates as $\Delta I > 0$, while the SEI dominates as $\Delta I < 0$. Therefore, the OBIRCH and SEI techniques have very similar response times from Figure 10. This conclusion is in accord with the predictions of the comprehensive model also because ΔI is proportional to ΔT.

3.2.4. The Relationship between Current Variation and Voltage Bias

Adjusting the voltage bias conditions V_0, ΔI will generate a series of complex changes (Figure 11a). As mentioned above, there exists a critical voltage V_c = 1.94 V.

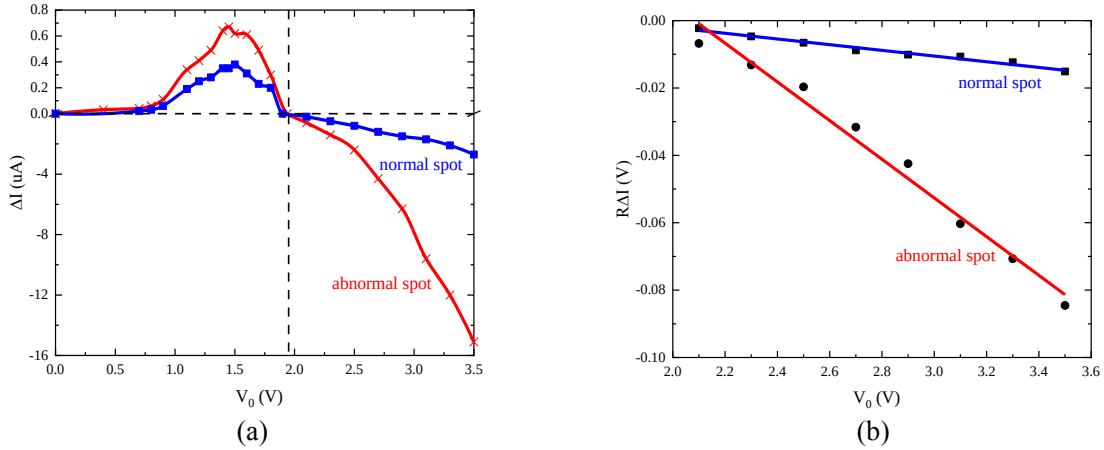


Figure 11. Curve of the current variation and the bias voltage: (**a**) $\Delta I \sim V_0$; (**b**) $R\Delta I \sim V_0$.

When V_0 is set between 1.8 V and 3.5 V, the OBIRCH technique dominates, and ΔI is negative. According to Equation (16), the contribution of OBIRCH, $-\frac{V_0}{R^2}\Delta R$, is proportional to V_0 and inversely proportional to R^2. Next, the resistance R decreases as the bias voltage V_0 increases (Figure 4b). Besides, ΔV_S is invariable because the Seebeck voltage is only related to the temperature gradient ∇T according to Equation (14). $\Delta R/R$ is also a constant because of the following formula:

$$\frac{\Delta R}{R} = \frac{\int \rho_0 \alpha_{\mathrm{TCR}} \frac{\Delta T}{A} \mathrm{d}l}{\int \rho_0 \frac{\mathrm{d}l}{A}} = \alpha_{\mathrm{TCR}} \overline{\Delta T} \tag{24}$$

where $\overline{\Delta T}$ is the average value of the temperature variation. Equation (13) is used in this formula. Therefore, the absolute value of ΔI's slope gradually increases as the V_0 increases. In order to find the values of ΔV_S and $\Delta R/R$, Equation (16) is modified to:

$$R\Delta I \approx \Delta V_S - \frac{\Delta R}{R} V_0 \tag{25}$$

The relationship between $R\Delta I$ and V_0 is shown in Figure 11b. After linear fitting, the values of ΔV_S and $\Delta R/R$ are calculated and listed in Table 4. These two values at Point A are much larger than those at Point B, showing that the thermal property at the abnormal spot is more sensitive than that at the normal spot. Besides, the critical voltage V_c can be calculated through Equation (17) using the data in Table 4, which is respectively 2.09 V at Point A and 1.75 V at Point B. These two values are close to the measured values V_c = 1.94 V.

Table 4. Values of ΔV_S and $\Delta R/R$.

	ΔV_S	$\Delta R/R$
Point A (abnormal spot)	0.120	0.0574
Point B (normal spot)	0.0148	0.00845

When V_0 is set between 0 V and 1.8 V, the SEI technique dominates, and ΔI is positive. Near 0 V (no bias applied), the resistance is so large that the value of ΔI tends to be zero. As the voltage increases, the resistance reduces, causing an increasing ΔI. In this period, OBIRCH's contribution is still small. At about 1.5 V (Figure 11a), ΔI is most affected by the SEI. After that, ΔI starts to fall.

In general, although the comprehensive model has many shortcomings, such as the inability to describe the temperature variation in the z direction, the inability to describe the temperature field evolution with different structures of the IC, the infinite increase of the temperature when the scanning velocity is zero, etc., it fits well with the experimental results. An in-depth study on the optimization of the comprehensive model is under way.

4. Conclusions

A theoretical comprehensive model of the TLS technique is proposed. The model quantitatively explains the experimental results in TLS technology.

Firstly, it shows that after the laser irradiation, the temperature variation has a positive correlation with the laser power and a negative correlation with the scanning velocity. Since the current variation is proportional to the temperature variation, it also meets these correlations.

Secondly, the response curve of the current variation is similar to the temperature response curve. A high coefficient $k = \frac{\kappa}{\rho c}$ at the abnormal spot of the DUT leads to a faster response rate than that at the normal spot. Besides, the response times in the OBIRCH and SEI techniques are almost equal. Therefore, these two techniques can be switched simply by adjusting the voltage bias.

Finally, the resistivity variation and the Seebeck voltage are generated together with the temperature field. At constant voltage bias, these two effects have opposite contributions to the current variation. As voltage varies, the current variation ΔI can be positive or negative under the laser irradiation. To get more precise results in the testing process, a high voltage bias should be used in the OBIRCH technique. Similarly, a high current bias should be used in the TIVA technique. Conversely, the SEI technique requires a low bias condition.

Author Contributions: Conceptualization, Y.L. and H.W.; Formal analysis, H.Y.; Investigation, H.Y.; Methodology, H.Y.; Project administration, R.C.; Resources, Y.M.; Supervision, J.H.; Validation, Y.L.; Writing—original draft, H.Y.; Writing—review & editing, R.C. and J.H. All authors have read and agreed to the published version of the manuscript.

Funding: This project was supported by Beijing Municipal Commission of Science and Technology (Grant No. E039360101).

Conflicts of Interest: The authors declare no conflict of interest.

References

1. Ross, R.J. *Microelectronics Failure Analysis: Desk Reference*, 6th ed.; ASM International: Materials Park, OH, USA, 2011.
2. Herfurth, N.; Wu, C.; Beyreuther, A.; Nakamura, T.; De Wolf, I.; Simon-Najasek, M.; Altmann, F.; Croes, K.; Boit, C. Non-invasive soft breakdown localisation in low k dielectrics using photon emission microscopy and thermal laser stimulation. *Microelectron. Reliab.* **2019**, *92*, 73–78. [CrossRef]
3. Lellouchi, D.; Lafontan, X.; Dhennin, J. MEMS Failure Analysis Case Studies Using the IR-OBIRCH Method-Short Circuit Localization in a MEMS. In Proceedings of the 2009 16th IEEE International Symposium on the Physical and Failure Analysis of Integrated Circuits, Suzhou, China, 6–10 July 2009.
4. Lin, H.S.; Wu, M.S. A case study of high temperature pass analysis using thermal laser stimulation technique. In Proceedings of the 2010 IEEE International Reliability Physics Symposium, California, CA, USA, 2–6 May 2010.
5. Beaudoin, F.; Imbert, G.; Perdu, P.; Trocque, C. Current leakage fault localization using back-side OBIRCH. In Proceedings of the 2001 8th International Symposium on the Physical and Failure Analysis of Integrated Circuits, Singapore, 13 July 2001.
6. Nordin, N.F. Application of Seebeck Effect Imaging on failure analysis of via defect. In Proceedings of the 2012 19th IEEE International Symposium on the Physical and Failure Analysis of Integrated Circuits, Singapore, 2–6 July 2012.
7. Beaudoin, F.; Desplats, R.; Boit, C. Principles of Thermal Laser Stimulation Techniques. *Microelectronics Failure Analysis: Desk Reference*; ASM Internationall: Materials Park, OH, USA, 2004; pp: 417–425.
8. Desplats, R.; Beaudoin, F.; Perdu, P.; Poirier, P.; Tremouilles, D.; Bafleur, M.; Lewis, D. Backside Localization of Current Leakage Faults Using Thermal Laser Stimulation. *Microelectron. Reliab.* **2001**, *41*, 1539–1544. [CrossRef]
9. Jacobs, K.J.P.; Wang, T.; Stucchi, M.; Gonzalez, M.; Croes, K.; De Wolf, I.; Beyne, E. Lock-in thermal laser stimulation for non-destructive failure localization in 3-D devices. *Microelectron. Reliab.* **2017**, *76*, 188–193. [CrossRef]
10. Nikawa, K.; Inoue, S. New Capabilities of OBIRCH Method for Fault Localization and Defect Detection. In Proceedings of the 6th Asian Test Symposium (ATS'97), Akita, Japan, 17–18 November 1997.
11. Cole, E.I., Jr.; Tangyunyong, P.; Benson, D.A.; Barton, D.L. TIVA and SEI developments for enhanced front and back-side interconnection failure analysis. *Microelectron. Reliab.* **1999**, *39*, 991–996. [CrossRef]
12. Beaudoin, F.; Chauffleur, X.; Fradin, J.P.; Perdu, P.; Desplats, R.; Lewis, D. Modeling Thermal Laser Stimulation. *Microelectron. Reliab.* **2001**, *41*, 1477–1482. [CrossRef]
13. Brahma, S.K.; Boit, C.; Glowacki, A. Seebeck Effect Detection on Biased Device without OBIRCH Distortion Using FET Readout. *Microelectron. Reliab.* **2005**, *45*, 1487–1492. [CrossRef]
14. Giowacki, A.; Boit, C. Characterization of thermoelectric devices in ICs as stimulated by a scanning laser beam. In Proceedings of the 2005 IEEE International Reliability Physics Symposium, San Jose, CA, USA, 17–21 April 2005.
15. Sanchez, K.; Desplats, R.; Beaudoin, F.; Perdu, P.; Dudit, S.; Vallet, M.; Lewis, D. Dynamic Thermal Laser Stimulation Theory and Applications. In Proceedings of the 2006 IEEE International Reliability Physics Symposium Proceedings, San Jose, CA, USA, 26–30 March 2006.
16. Bray, J.W. *Metals Handbook, vol 2: Properties and Selection: Nonferrous Alloys and Special-Purpose Materials*, 10th ed.; ASM International: Materials Park, OH, USA, 1990.
17. Dizaji, A.F.; Jafari, A. Three-dimensional fundamental solution of wave propagation and transient heat transfer in non-homogenous media. *Eng. Anal. Bound. Elem.* **2009**, *33*, 1193–1200. [CrossRef]

18. Naoe, T.; Mizobe, T.; Yokoyama, K. Case studies of defect localization based on software based fault diagnosis in comparison with PEMSOBIRCH analysis. *Microelectron. Reliab.* **2014**, *54*, 1433–1442. [CrossRef]

Publisher's Note: MDPI stays neutral with regard to jurisdictional claims in published maps and institutional affiliations.



© 2020 by the authors. Licensee MDPI, Basel, Switzerland. This article is an open access article distributed under the terms and conditions of the Creative Commons Attribution (CC BY) license (http://creativecommons.org/licenses/by/4.0/).